ACS APPLIED MATERIALS & INTERFACES

Research Article

www.acsami.org

Facile Aerosol Synthesis and Characterization of Ternary Crumpled Graphene–TiO_2–Magnetite Nanocomposites for Advanced Water Treatment

Yi Jiang, Wei-Ning Wang, Pratim Biswas,* and John D. Fortner*

Department of Energy, Environmental, and Chemical Engineering, Washington University in St. Louis, St. Louis, Missouri 63130, United States

Supporting Information

ABSTRACT: In this work, the synthesis and characterization of multifunctional crumpled graphene-based ternary nanocomposite photocatalysts for advanced water treatment applications is described. Currently, a major hurdle for the scale-up and optimization of aqueous, graphene-based photocatalysts is restacking of graphene nanosheets due to strong $\pi-\pi$ interactions. To overcome this hurdle, a fast and facile aerosol technique to synthesize monomeric, aggregation-resistant, crumpled graphene-based photocatalysts was developed. The aerosol route utilizes water evaporation-induced confinement forces to effectively crumple graphene oxide and subsequently encapsulate commercially available TiO_2 and magnetite nanoparticles. The as-synthesized crumpled graphene–TiO_2–magnetite (GOTIM) ternary core–shell nanostructures are shown to possess superior aqueous-based photocatalytic properties (over a 20-fold enhancement in some cases) compared to TiO_2 alone. Total GOTIM photocatalytic reactivity is confirmed to also include efficient photoreduction reaction pathways, in addition to expected oxidation routes typical of TiO_2-based photocatalysts, significantly expanding photocatalytic application potential compared to TiO_2 alone. Reaction kinetics and proposed mechanisms (both oxidative and reductive) are described for a model organic compound, here as methyl orange. Further, with the addition of hole scavengers such as EDTA, and/or lowering the O_2 concentration, we demonstrate enhancement of photocatalyzed reduction reactions, suggesting potential for directed, controlled reduction applications. In addition to robust aqueous stability, low-field magnetic susceptibility is demonstrated, allowing for low-energy, *in situ* material separations, which are critical for material recycling and reuse.

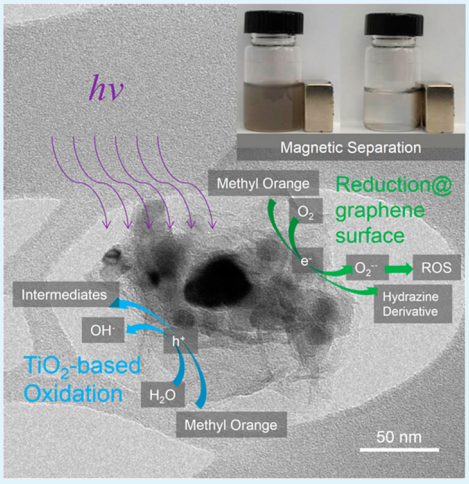

KEYWORDS: *crumpled graphene, TiO_2, magnetite, photocatalyst, ternary nanostructure, water treatment, nanocomposite*

INTRODUCTION

Water treatment using photocatalysts, particularly TiO_2, has garnered considerable attention and been successfully demonstrated in a number of applications.[1,2] Recent material advances with combined TiO_2–carbon nanomaterial-based photocatalysts, such as graphene and carbon nanotubes, have demonstrated superior and sometimes unique physical and chemical properties compared to traditional analogs. For example, fullerene (C_{60})-incorporated TiO_2 nanorods demonstrated enhancement of photocatalytic activity by nearly 2.7 times compared to Degussa P25,[3] whereas carbon nanotube (CNT)–TiO_2 materials also demonstrated enhanced activity with rates dependent on dopant ratios (maximum oxidation rates were found at ~85 wt. % CNT).[4] A hybrid P25–graphene composite material, synthesized via a one-step, hydrothermal method, was demonstrated to be a superior photocatalyst compared to bare P25 (measured by the degradation rate of methylene blue) due to increased light absorption range, more pollutant adsorption (surface localization) and decreased recombination of photoinduced holes and electrons.[5] Further, graphene-based TiO_2 photocatalysts may eventually prove to be economical, as they are not only more efficient per unit mass when compared to traditional analogs, but also composed of abundant, available and relatively low cost elemental components in addition to rapidly decreasing graphene production costs. To date, one of the significant issues in the aqueous-based processing and applications of graphene composites lies in the material's tendency to restack due to strong $\pi-\pi$ attractions between graphene nanosheets.[6] Restacking results in significant decreasing of accessible surface area and aqueous stability/accessibility, and thus loss of material efficacy over a short time.[7,8] To avoid restacking/instabilities, there have been a number of strategies employed such as spacer additions (e.g., CNT[9] and water[10]); however, the overall catalytic durability and reliable recovery (separation),

Received: April 25, 2014
Accepted: July 1, 2014
Published: July 1, 2014

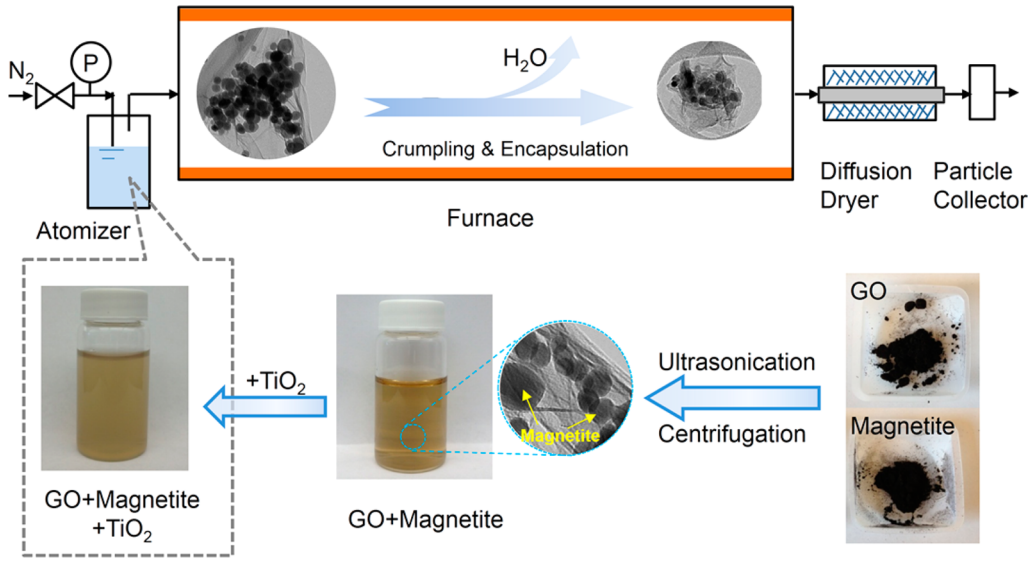

Figure 1. Experimental setup. Schematic diagram of a FuAR and the synthesis process.

which both are needed for successful recycling/application strategies, for such materials has yet to be fully demonstrated.

Interestingly, there have been recent advancements in the development of three-dimensional (3D), nanoscale, graphene composite structures, which can be specifically engineered to avoid two-dimensional (2D) limitations stated above. Specifically, by "crumpling" graphene and graphene oxide, it has been observed that resulting 3D structures have outstanding compression- and aggregation-resistant properties in water.[6,8] Further, aggregation-resistant, crumpled graphene-nanocrystal composites can be synthesized via direct aerosolization starting with either graphene oxide suspensions mixed with precursor ions[11] or presynthesized nanoparticles, resulting in binary and ternary composite materials.[12,13] Such crumpled graphene-based nanocomposites, which have been demonstrated to include the incorporation of Si,[14] Pt,[15] Mn_3O_4 and SnO_2,[11] TiO_2,[16,17] Au/Fe_3O_4[13] (either through encapsulation or sack-cargo surface complexes), have been primarily evaluated for electrochemical and magnetic applications. However, as a high performance aqueous-based photocatalyst, crumpled graphene−TiO_2 structures have not yet been thoroughly evaluated. Additionally, tailoring crumpled graphene−TiO_2 magnetic susceptibility through the incorporation of magnetite nanoparticles, and thus allowing for simple catalyst recovery strategies, is of high interest for material reuse/recycle, particularly in a context of economically sustainable processing.

Crumpled graphene-based nanocomposites can be readily produced by an aerosol-based approach.[11,12] Briefly, graphene oxide precursors are aerosolized into micrometer-sized droplets by using a nebulizer and then delivered by N_2 into a furnace aerosol reactor (FuAR). During the flight time within the reactor, a single graphene oxide sheet effectively crumples under evaporation-induced confinement forces allowing for the effective encapsulation of associated nanoparticles, thus forming a core−shell type nanocomposite. The encapsulated nanocrystals can be presynthesized nanoparticles (e.g., citrate-stabilized Ag nanoparticles),[12] or grown from precursor ions.[11] Combined, the graphene oxide sheets and precursor content, either presynthesized nanoparticles or precursor ions, determine the size and composition, thus functionality, of the resulting material. For example, magnetic susceptibility can be achieved and tuned by incorporating a magnetic precursor component such as nanoscale magnetite (Fe_3O_4) particles, as described in this work.

Previous research describing (flat) graphene−TiO_2 photocatalytic reactions have primarily focused on oxidation pathways.[5,18−21] Under UV irradiation (<380 nm wavelength) photoinduced holes (h^+) and radical species, such as superoxide radicals ($O_2^{-}\cdot$) and hydroxyl radicals (OH·), can oxidize model target species or pollutants.[18,21] Targeted photocatalytic reduction of pollutants, such as U(VI),[22] Cr(VI),[23,24] Cu(II),[25] 2,4,6-trinitrotoluene (TNT)[26] and CO_2,[27] has not, however, been a focus area to date for graphene−TiO_2 structures despite the possibility of engineering reduction pathways as induced electrons lifetime and occurrence can be significantly enhanced under UV irradiation.[18] Based on this, a detailed exploration of both oxidation and reduction reaction pathways for photoinduced holes and excited electrons, uniquely enabled through engineered, crumpled graphene−TiO_2 materials for aqueous catalytic redox processes, is needed.

This work focuses on two significant aspects of crumpled graphene−TiO_2 aqueous photocatalysts: (1) synthesis and evaluation of a new ternary crumpled graphene (or reduced graphene oxide)−TiO_2−magnetite (GOTIM) photocatalysts, which are highly stable, aggregation-resistant and magnetically recoverable in water; and (2) identification and exploration of extended aqueous reaction pathways for (UV) photoinduced holes and electrons for synthesized materials, including the enhancement of photocatalytic reduction-based reactions. Together, this works highlights the platform potential for crumpled graphene−TiO_2 photocatalysts to be broadly multifunctional, including the extension of reaction regimes, in addition to being recoverable via low magnetic fields, allowing for simple yet efficient separation/reuse strategies.

EXPERIMENTAL SECTION

Precursor Preparation. Graphene oxide (GO) was synthesized using the modified Hummers method[28] and was reported in our previous work.[8] To obtain the GOTIM ternary nanocomposite, dry GO powder (200 mg) and commercial magnetite nanoparticles (primary size <50 nm, Sigma-Aldrich, 100 mg) were premixed and dispersed in 200 mL of water and ultrasonicated for 1 h using a microtip sonicator (Qsonica). This process allows the exfoliated GO

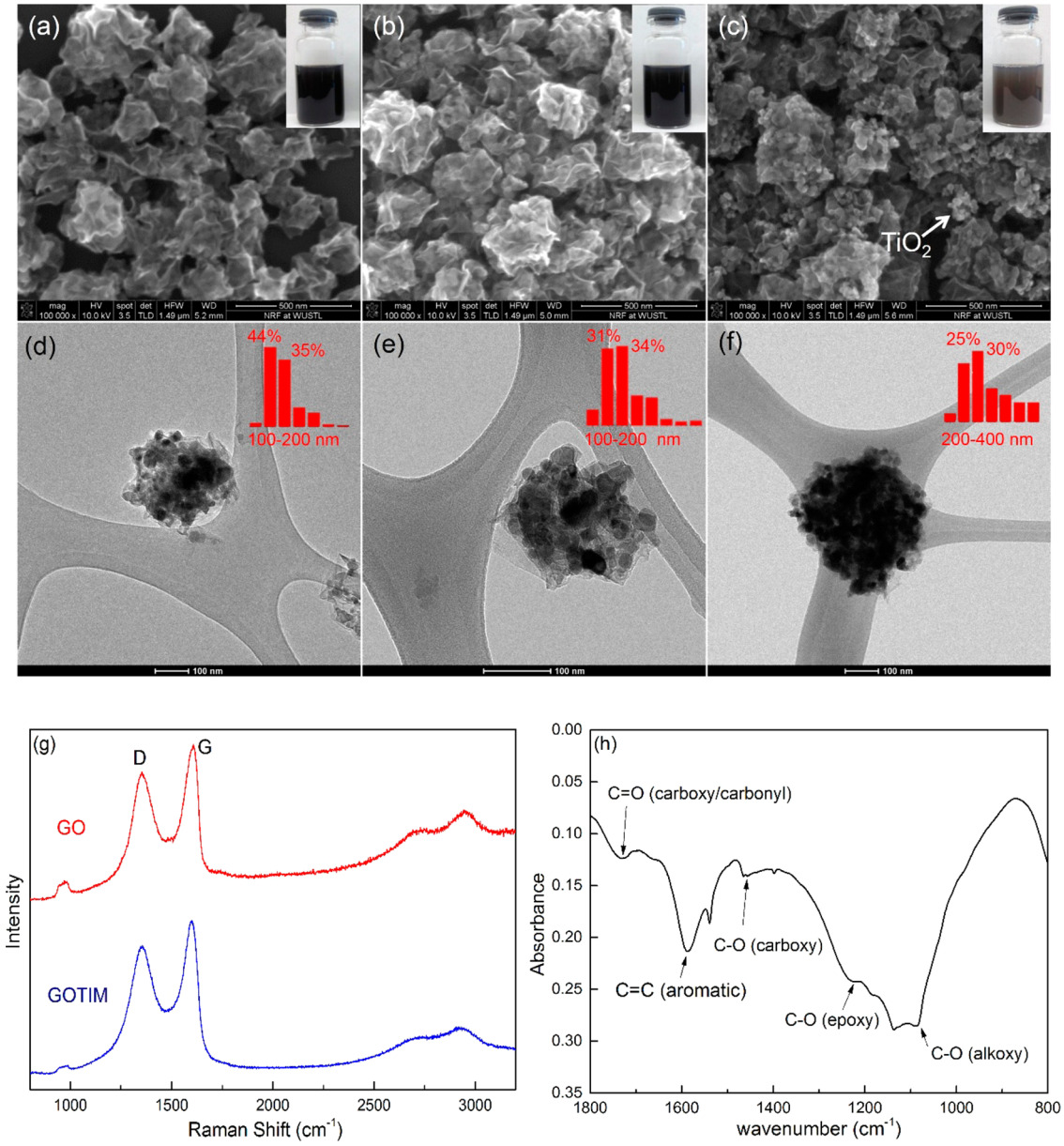

Figure 2. GOTIM with different TiO_2 contents. (a–c) SEM images of GOTIM-A, GOTIM-B and GOTIM-C as well as digital photos of corresponding dispersions in the insets (200 mg/L). (d–f) TEM images of GOTIM-A, GOTIM-B and GOTIM-C, with corresponding number-based PSD from DLS in the insets. The two percentages correspond to the highest two peaks. (g) Raman spectra of flat GO and GOTIM-B. (h) FTIR spectrum of GOTIM-B.

nanosheets to associate with disaggregated magnetite nanoparticles. The suspension was then centrifuged at 10 000 rpm for another 1 h. The supernatant, with exfoliated GO nanosheets and attached magnetite nanoparticles, was then added with TiO_2 nanoparticles at different weight percentages (Evonik Degussa Aerodisp; 7, 14, 28 mg) and aerosolized (Figure 1). Crumpled graphene–TiO_2 (GOTI) nanocomposite was also synthesized for the photocatalytic reaction experiments. To obtain the GOTI nanocomposite, GO solution was directly mixed with TiO_2 (28 mg of TiO_2 into 200 mL of GO solution); and the mixture was then aerosolized.

Crumpled Graphene Nanocomposite Synthesis. To obtain the crumpled graphene nanocomposite, a furnace aerosol reactor (FuAR) was utilized (Figure 1). The precursor solution was atomized into micrometer-sized droplets by using a Collison nebulizer (BGI Incorporated), and then delivered by N_2 into tubular alumina reactor (1 m × 25 mm ID) maintained at 400 °C, to enable the successful crumpling of GO, yet partially preserve the functional groups, such as carboxyl and hydroxyl groups that are critical for nanocomposite stability in water due to electrostatic repulsion.[8] The flow rate was operated at 12.4 L/min by adjusting the nebulizer pressure (14 psi, 96.53 kPa), resulting in ~1.6 s residence time. During the flight in the furnace, graphene oxide became crumpled under the evaporation-induced confinement force and could effectively encapsulate nanoparticles dispersed in the precursor solution.[12] Finally, the nanocomposites were collected downstream of the reactor, weighed and dispersed into water to obtain 200 mg/L dispersion.

Nanoparticle Characterization. The optical properties of GOTIM aqueous dispersions (200 mg/L) were measured by using a UV–vis spectrophotometer (Varian Bio 50). The ζ-potential and hydrodynamic diameter of aqueous GOTIMs were measured using Zetasizer Nano ZS system (Malvern Instruments). The morphology and size of the GOTIM nanoparticles were also examined by field emission scanning electron microscopy (FESEM, NOVA NanoSEM 230), transmission electron microscopy (TEM, Tecnai TM Spirit) and high resolution-TEM (HR-TEM, JEOL 2100). The crystal phase was determined by X-ray Diffraction (XRD) (Geigerflex D-MAX/A,

Rigaku Denki) with Cu Kα radiation (λ = 1.548 Å). The GOTIM nanoparticles were digested in concentrated HNO_3 at 110 °C for 10 h and diluted for inductively coupled plasma mass spectrometry (ICP-MS, Agilent 7500cc) analysis to quantify the TiO_2/magnetite ratios. GOTIM nanocomposite molecular bond and functionality analyses were performed via Raman spectrometry (Renishaw InVia Reflex confocal Raman spectrometer with a 514 nm laser) and Fourier transform infrared spectrometry (FTIR, Nicolette Nexus 470).

Photodegradation of a Model Dye. The photocatalytic activity of synthesized GOTIMs was evaluated by the photodegradation of a model pollutant, methyl orange (MO). Typically, 50 mL of MO solution (C_0 = 9.6 or 20 mg/L) and GOTIM photocatalyst (8 or 16 mg/L, suspended) was added into a quartz beaker. A xenon lamp (with intensities of 14.4 or 18.8 mW/cm^2 in the effective UV range (250−387 nm)) was used as the irradiation light source; and an overhead stirrer was used to promote mass transfer in the solution. The distance between the center of the beaker and the light source was set to be 16 cm. Before each reaction, the solution was stirred in the dark for 30 min to achieve adsorption equilibrium. During the reaction, 2 mL of sample was collected at each time interval (10 min) and filtered using a syringe filter (Millex PES, 0.22 μm) before UV−vis measurement to determine the remaining MO concentration at the absorption peak 463 nm. Photodegradation of MO using bare TiO_2 nanoparticles was also conducted under the same conditions for comparison.

Identifying Reaction Pathways. To help identify and explore major reaction pathways, *tert*-butanol (*t*-BuOH, 10 mM, Sigma-Aldrich),[29,30] catalase (500 units/mL, Sigma-Aldrich)[31] and ethylenediaminetetraacetic acid (EDTA, 4 mM, Sigma-Aldrich)[32] were employed as OH·, H_2O_2, and h^+ scavengers, respectively. For anaerobic reactions, a capped quartz serum bottle was used instead and the solution was purged with N_2 for 30 min before the photocatalytic reactions.

Reuse/Cycling Experiments. To evaluate recycling potential and material reuse, after each reaction cycle (beginning with a batch reaction as described above), a specified amount of MO stock solution (C = 500 mg/L) was added to keep $[MO]_0$ = 10 mg/L at the beginning of next reaction. After five cycles, the remaining GOTIM was collected using a magnet (ca. 1T neodymium, Applied Magnets) and the collection efficiency was calculated from the difference between the GOTIM UV−vis absorbance (320 nm) before and after the cyclic experiments.

RESULTS AND DISCUSSION

Material Synthesis and Characterization. For materials described, the desired ternary crumpled GOTIM nanocomposite requires precursors containing three components, graphene oxide sheets, TiO_2 and magnetite together, either in the (original) form of presynthesized nanoparticles or precursor ions. The former (presynthesized nanoparticle) approach was chosen not only because of commercial availability of nanoscale TiO_2 and magnetite but also because precursor ions can lead to incomplete growth and heterogeneous distribution of TiO_2 and magnetite in the resulting composites.

Previous research highlights the key role of aqueous stability regimes (particularly electrostatic interactions between graphene nanosheets and nanoparticles) in determining the success of synthesis of GO-based ternary nanostructures.[13] Graphene oxide is stable in water with a ζ-potential usually being <−30 mV;[33] and TiO_2 can be prepared as an aqueous dispersion (Degussa). However, untreated/uncoated, commercial magnetite nanoparticles (Sigma-Aldrich, <50 nm) are not readily water-dispersible, based on high particle surface energies, preventing direct, homogeneous atomization. Here, the aerosol-based technique was thus modified to first anchor magnetite nanoparticles onto GO nanosheets. By sonicating an aqueous mixture of GO and magnetite nanoparticles, successful surface attachment of magnetite nanoparticles with GO took place, as shown in the TEM graph in Figure 1. It was observed that the commercially available magnetite nanoparticles were poly-dispersed, with diameters ranging from 10 to 50 nm, and either coupled onto the GO nanosheet surface or crumpled edges. Previous research reports that nanoparticles can interact with the GO nanosheets via various physical and chemical interactions, such as physisorption, electrostatic binding and charge transfer interactions.[34−37] In this work, the ζ-potentials measured from electrophoretic light scattering, show an increasing ζ-potential for GO−magnetite dispersion (−28 mV), as compared with pure GO solution (−48 mv), indicating electrostatic binding may facilitate the attachment of magnetite nanoparticles (thus lessening the total particle surface charge). Additionally, the point of zero charge (PZC) of magnetite ~7, as reported in other's work,[13] also provided support for the electrostatic binding mechanism, as the GO solution used in this work has a pH ~3. As produced, the GO-magnetite dispersion was next mixed with a TiO_2 aqueous suspension (varying concentration of TiO_2), then atomized and finally delivered by N_2 (flow rate 12.4 L/min) into the reactor (400 °C), producing crumpled GOTIM composites (Figure 1).

Crumpled GOTIM nanocomposites were collected using a membrane filter (Millipore ISOPORE, 0.2 um) downstream of the reactor and characterized. Figure 2a−f shows digital photos, FESEM, TEM as well as number-based, particle size distribution (PSD) of synthesized GOTIM with three TiO_2/magnetite ratios (as calculated from ICP-MS measurements of acid digested samples, 1.8, 1.9 and 2.7, and denoted as GOTIM-A, -B and -C, respectively, hereafter). GOTIM dispersions are black, indicating GO being partially thermally reduced with graphene regions at 400 °C (insets of Figure 2a,b), which has been observed previously.[38] Quasi-spherical, core−shell (also termed sack-cargo) nanostructures were observed for all GOTIMs as shown in Figure 2a,b,c.[12] With the increase of interior particle volume (number/size), surface roughness was observed to decrease with visual identification of incorporation of TiO_2 and magnetite nanoparticles, which increased with higher (interior) loading ratios (from Figure 2a−c). For GOTIM-C, which has the highest TiO_2 mass loading, incomplete encapsulation of all TiO_2 nanoparticles was observed. For this case, TiO_2 nanoparticles also aggregated on the outer surface of GO, as indicated by the white arrow in Figure 2c. High TiO_2 mass loading was also reflected in the gray color of GOTIM-C dispersion (Figure 2c inset), compared to much darker suspensions for Figure 2a,b. Figure 2d,e,f show corresponding TEM images of GOTIM, with number-based PSD derived from dynamic light scattering (DLS) measurements in the insets. These TEM micrographs further confirmed the material structure as a crumpled GO shell, with TiO_2 and magnetite coexisting as the core. Further, HR-TEM analysis reveals that TiO_2 nanoparticles have an orientation of anatase (101) plane, whereas magnetite nanoparticles reveal an orientation of (111) plane (Figure S1, Supporting Information). In addition, XRD analysis of GOTIM and CGO was performed (Figure S2, Supporting Information) and when compared with CGO alone, TiO_2 and magnetite diffraction patterns were observed in GOTIM samples. It was also observed from the PSD data that the peak size of the nanocomposite increased from 100 to 200 nm to 200−400 nm with the encapsulation of more TiO_2 nanoparticles. This demonstrates that by employing an improved synthesis strategy (first GO−magnetite solution, then adding TiO_2 aqueous

dispersion), instead of sonicating a pot of three components together (GO, magnetite, TiO_2),[13] GOTIM nanocomposites of tunable size and functionality can be readily achieved. Raman analysis of GOTIM-B shows the two characteristic bands of GO, D band (~1350 cm^{-1}, measuring hexagonal carbon pattern distortions, such as defects) and G band (~1600 cm^{-1}, pure sp^2 hybridized graphitic carbon). The ratio of D and G band intensities (I_D/I_G) for these samples remains virtually unchanged after aerosol (and thermal) processing (from 0.84 (flat GO) to 0.85 (GOTIM)), indicating an optimal balance of synthesis (crumpling) conditions while maintaining hydrophilicity (via surface oxidation). CGO FTIR spectrum in Figure 2h indicates a mixture of oxygen-based functional moieties present including C—O (alkoxy), C—O (epoxy), C—O (carboxy), C═C (aromatic), and C═O (carboxy/carbonyl) stretches.[39]

The UV−vis absorption spectra of GOTIM demonstrate a red shift with increasing TiO_2 content (e.g., ca. 20 nm shift for GOTIM-C compared to bare TiO_2) and for all GOTIM materials described, an extended absorption range was observed when compared to bare TiO_2, which is due to the band gap narrowing of TiO_2 when participating in Ti−O−C interactions.[40,41] This red shift enables the more efficient utilization of the solar spectrum and has been observed previously for flat graphene−TiO_2 nanocomposite (see Figure S3, Supporting Information).[5,18] As described, all materials had a net negative surface charge ($\zeta_{GOTIM\text{-}A}$ = −46.6 mV, $\zeta_{GOTIM\text{-}B}$ = −48.7 mV, $\zeta_{GOTIM\text{-}C}$ = −41.0 mV) providing aqueous stability. No significant sedimentation was observed for months for GOTIM-A and GOTIM-B. For GOTIM-C, which had excess TiO_2 on the composite surface, partial sedimentation was observed after 1 month.

GOTIM Photocatalytic Characterization. The mechanism of graphene enhanced TiO_2 photocatalytic performance is hypothesized to be, in essence, the same for other carbon-TiO_2 structures, such as carbon nanotubes, fullerenes and activated carbon. Specifically, photocatalytic enhancement for these previously studied materials was proposed to result from an increased light absorption range, more pollutant adsorption and decreased recombination of photoinduced holes and electrons.[5,18] However, how crumpled graphene (in contrast to 2D flat analogs) can specifically alter TiO_2's photocatalytic activity has not been assessed. Here we evaluated the simple photodegradation of methyl orange, a model organic dye,[32,42,43] under a xenon lamp irradiation (14.4 mW/cm^2 in the effective UV range (250−387 nm)). A typical photodegradation kinetic analysis, using GOTIM-B as an example material, is shown in Figure 3. Although the TiO_2 mass ratio was significantly reduced (TiO_2 wt./total wt.:12.1%) compared to pure TiO_2 (100%); GOTIM-B still outperformed TiO_2 under the same conditions. For example, after a 90 min reaction in the case of 20 mg/L MO and 16 mg/L catalysts, ~ 41% and ~28% MO remained in the solution for TiO_2 and GOTIM-B respectively. Consistent with previous reports, agreeable fitting of pseudo-first-order kinetic parameters suggested a pseudo-first-order reaction (R^2 = 0.978−0.999) (see Table S1, Supporting Information).[21]

The reaction rate constants for TiO_2 and GOTIM are further compared in Figure 4. The direct observed enhancement factor for GOTIM-A, -B and -C are 1.1, 1.2 and 2.9, respectively, when compared to bare TiO_2, whereas normalized to TiO_2 mass, the enhancement reached a >20 fold enhancement (GOTIM-C), demonstrating (further) enhanced material

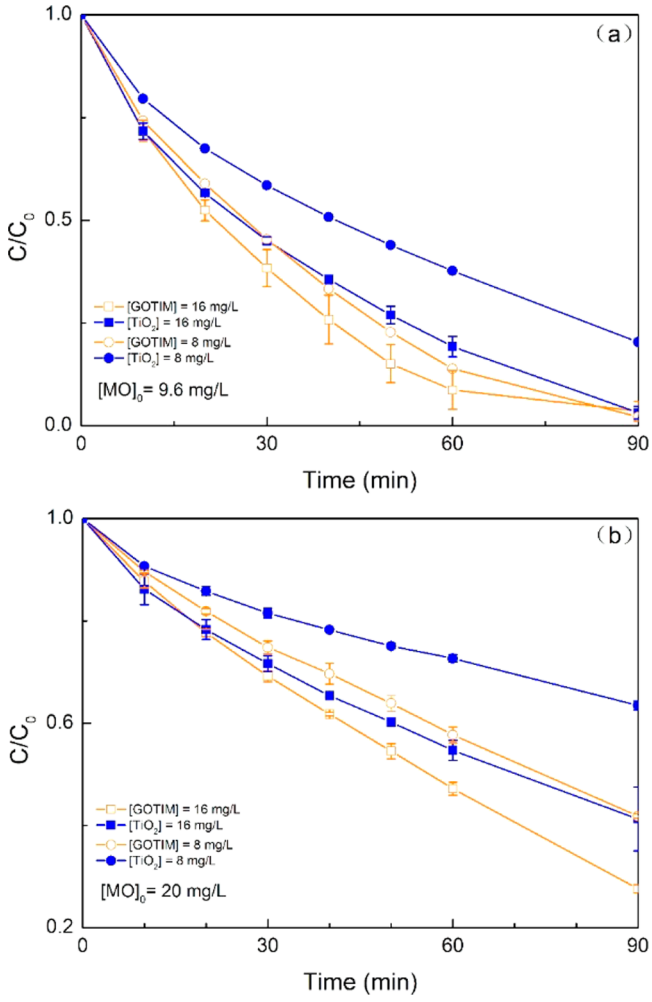

Figure 3. Methyl orange concentration (C/C_0) with time in the presence of GOTIM-B and TiO_2 under xenon lamp irradiation (light intensity = 14.4 mW/cm^2 in the 250−387 nm region) (□, [GOTIM] = 16 mg/L; ■, [TiO_2] = 16 mg/L; ○, [GOTIM] = 8 mg/L; ●, [TiO_2] = 8 mg/L).

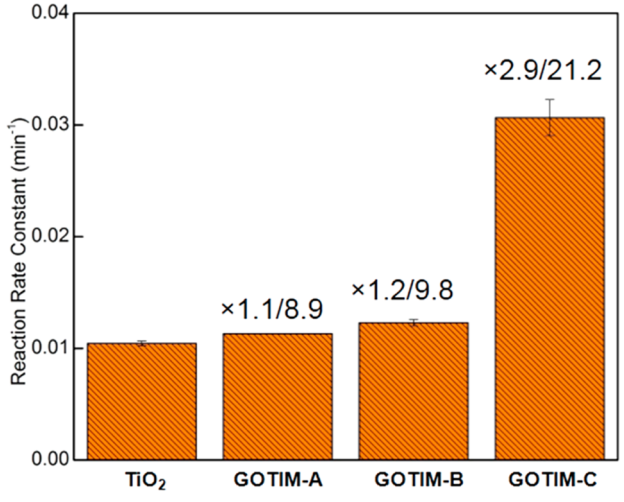

Figure 4. Comparison of reaction rate constants of GOTIMs. $[MO]_0$ = 20 mg/L, [catalyst] = 16 mg/L; light intensity = 14.4 mW/cm^2 (250−387 nm). The enhancement factors on the right were ones normalized by TiO_2 ratios. TiO_2/magnetite ratios are 1.8, 1.9 and 2.7, for GOTIM-A, -B and -C, respectively.

photocatalytic efficacy. This trend is in good accordance with the TiO_2/magnetite ratios (as calculated from ICP-MS results, 1.8, 1.9 and 2.7, respectively), which implicate the key role of TiO_2 in determining (and engineering) GOTIM photocatalytic performance. Meanwhile, crumpled graphene−TiO_2 (binary GOTI) was found to have a 4.5 times direct enhancement in performance compared with bare TiO_2 (see Figure S4, Supporting Information). Such performance enhancement is comparable to recent reports of flat graphene−TiO_2 nanocomposites, which ranges from 2.5 to 8.5 times.[19,20,44] In addition, experimental results also show that increased light intensity (18.8 mW/cm^2 in the effective UV range (250−387 nm)) enhances the photocatalytic activity in a differential manner, indicating that GOTIM is more sensitive to light intensity than bare TiO_2 (e.g., 2.5 and 1.8 times enhancement for GOTIM-B and TiO_2, respectively, with increased light intensity) (see Figure S4, Supporting Information).

Reuse and Recovery of GOTIM. The reuse or recyclability, measured by the photodegradation of methyl orange for five consecutive cycles (t_R = 60 min), was evaluated. After each cycle, a specified amount of MO stock solution (500 mg/L) was added to maintain $[MO]_0$ = 10 mg/L at the beginning of each cyclic experiment. For the first cycle, after a 60 min reaction time, 98% methyl orange was observed to be degraded; and for the fifth cycle, although only 85% remaining (of initial mass) GOTIM-B photocatalyst participated in the reaction (due to 4% sampling loss per cycle), MO removal has still reached 91% (see Figure S5, Supporting Information), indicating catalytic stability under these conditions. After five cycles, GOTIM-B was separated and collected from the remaining solution by using a hand-held, neodymium magnet (Applied Magnets). For the remaining GOTIM-B photocatalyst, ∼50−60% could be recovered with a low magnetic field, which decreased from a >90% recovery rate before reaction cycling. This may be attributed to the dissolution of iron ions during the reaction[13] (which may undergo redox-based reactions in proximity with TiO_2) and is currently being further investigated. Collected (GOTIM-B) nanoparticles did maintain aqueous (monomeric) stability after being redispersed into water (ζ = −30.5 mV).

Enhanced TiO_2-based Photocatalytic Reduction Pathways. The photocatalyzed, oxidative reaction mechanisms of TiO_2 have been extensively described in literature reports. To summarize, TiO_2 as a semiconductor produces electron−hole pairs upon UV irradiation with energies greater than its band gap (3.2 eV) (eq 1).[34] The photoinduced hole−electron pairs are separated in the space-charge layer, and can lead to oxidation and reduction reactions, respectively, due to their strong redox potentials (valence band hole: 2.5 V vs SCE and conduction band electron: −0.7 V vs SCE).[42] The photoinduced holes can then directly oxidize pollutant, or oxidize water to produce hydroxyl radicals (OH·), whereby indirect oxidation (by OH·) takes place (eq 2). Interestingly, when in contact with graphene (in either binary or ternary structures), which exists as an electron acceptor, an overall decrease in recombination kinetics of separated holes and electrons has been observed, leading to increased reactions (availability) of holes and radicals.[18] Direct oxidation by holes and indirect oxidation by formed radicals is widely considered to be the main (oxidation) reaction mechanism for pollutant degradation.[18,21]

Compared to oxidation reactions, less attention has been given to the increase in electron production for such systems, which could potentially promote strong reduction reactions for TiO_2-based systems/materials. In this work, methyl orange also serves as a probe for resulting reduction reactions based on a more positive reduction potential (−0.28 V vs SCE) when compared with the conduction band electrons (−0.7 V vs SCE).[45] Here, it was observed that graphene−TiO_2 has a significantly stronger photocatalytic reduction capacity when compared to pure TiO_2. A new absorption peak (247 nm), characteristic of the reduced product of methyl orange, a hydrazine derivative,[43] appears for irradiated reactions with GOTIM-B, whereas such a peak was not obvious for bare irradiated TiO_2 (Figure 5a,b) (eq 3). This peak (or concentration of reduced product) was further increased by depleting O_2, as shown in Figure 5c. Figure 5 insets show the evolution of the reduced product concentration (absorbance at 247 nm) in the first 60 min. The highest absorbance for GOTIM-B (Figure 5c inset) reaches ca. 3 times that of TiO_2 (Figure 5a inset), indicating the potential of GOTIM to also efficiently photocatalyze available reduction pathways (which was also evidenced by enhancement of photoreduction of CO_2 using crumpled graphene−TiO_2 photocatalyst in our other work[17]). The enhancement of photocatalytic reduction reactions by depleting O_2 suggests a competing role of O_2 with MO for the photoinduced reducing electrons. One electron reduction of O_2 into a superoxide anion radical (O_2^-·) has a redox potential of −0.57 V vs SCE,[46] which is also more positive than that of conduction band electrons (eq 4). Similar production of O_2^-· was also reported in previous research.[18]

Furthermore, O_2^-· directly promotes the production of other reactive oxygen species (ROS), such as HO_2·, H_2O_2 and OH· (eqs 5−7).[42,47] To further confirm such reaction pathways for this system, a H_2O_2 scavenger, catalase, was employed,[31] which significantly slowed the reaction kinetics compared with no scavenger (Figure 6a), implicating peroxide involvement (of MO degradation) directly or in generation of other ROS species (which can then react). Further experiments with hydroxyl radical scavenger *t*-BuOH ($k_{[t\text{-BuOH+OH}\cdot]} = 5 \times 10^8$ M^{-1} s^{-1}; 10 mM) partially suppressed the degradation of MO as well (Figure 6b), suggesting that ROS species (from peroxide degradation or water) are involved in the MO degradation pathway(s) (eqs 2 and 7).

$$TiO_2 + h\nu \rightarrow TiO_2 + h^+ + e^- \quad (1)$$

$$h^+ + H_2O \rightarrow OH\cdot + H^+ \quad (2)$$

$$(CH_3)_2NC_6H_4N{=}NC_6H_4SO_3^- + 2H^+ + 2e \rightarrow (CH_3)_2NC_6H_4NHNHC_6H_4SO_3^-\cdot \quad (3)$$

$$e + O_2 \rightarrow O_2^-\cdot \quad (4)$$

$$O_2^-\cdot + H^+ \rightarrow HO_2\cdot \quad (5)$$

$$HO_2\cdot + O_2^-\cdot + H^+ \rightarrow H_2O_2 + O_2 \quad (6)$$

$$H_2O_2 + e \rightarrow OH\cdot + OH^- \quad (7)$$

The effect of hole scavengers on promoting reduction reactions was evaluated with EDTA, which has strong hole scavenging capacity, reacting with holes ca. 19 000 times faster than the recombination of holes and electrons.[32] As observed in Figure 6c, with the addition of EDTA, the absorbance at 247 nm (indicating reduced product) increased considerably at an

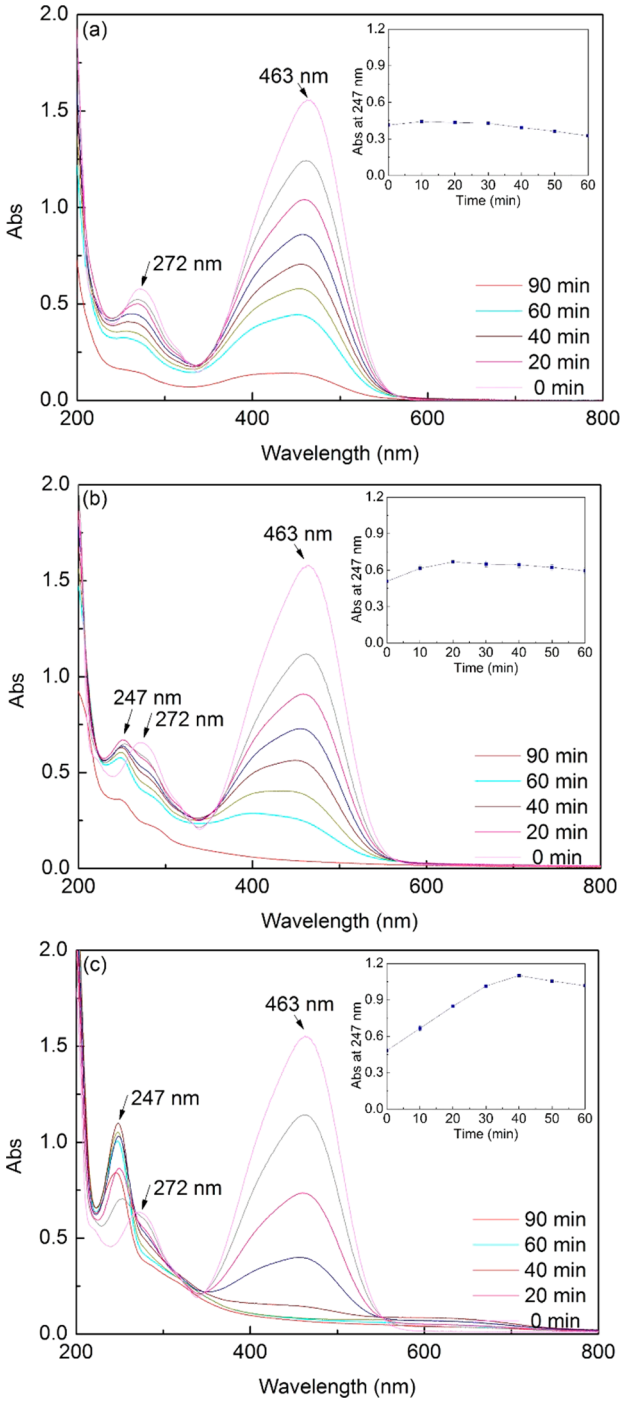

Figure 5. Evolution of UV−vis absorption spectrum of MO with time in the presence of (a) TiO_2 with O_2, (b) GOTIM-B with O_2 and (c) GOTIM-B without O_2. The insets show the evolution of absorbance at 247 nm (MO reduced product concentration), with the highest absorbance for GOTIM-B (c) reaching ca. 3 times that of TiO_2 (a), indicating the potential of GOTIM to also efficiently photocatalyze available reduction pathways. $[MO]_0$ = 20 mg/L; [catalyst] = 16 mg/L; light intensity = 18.8 mW/cm^2 (250−387 nm).

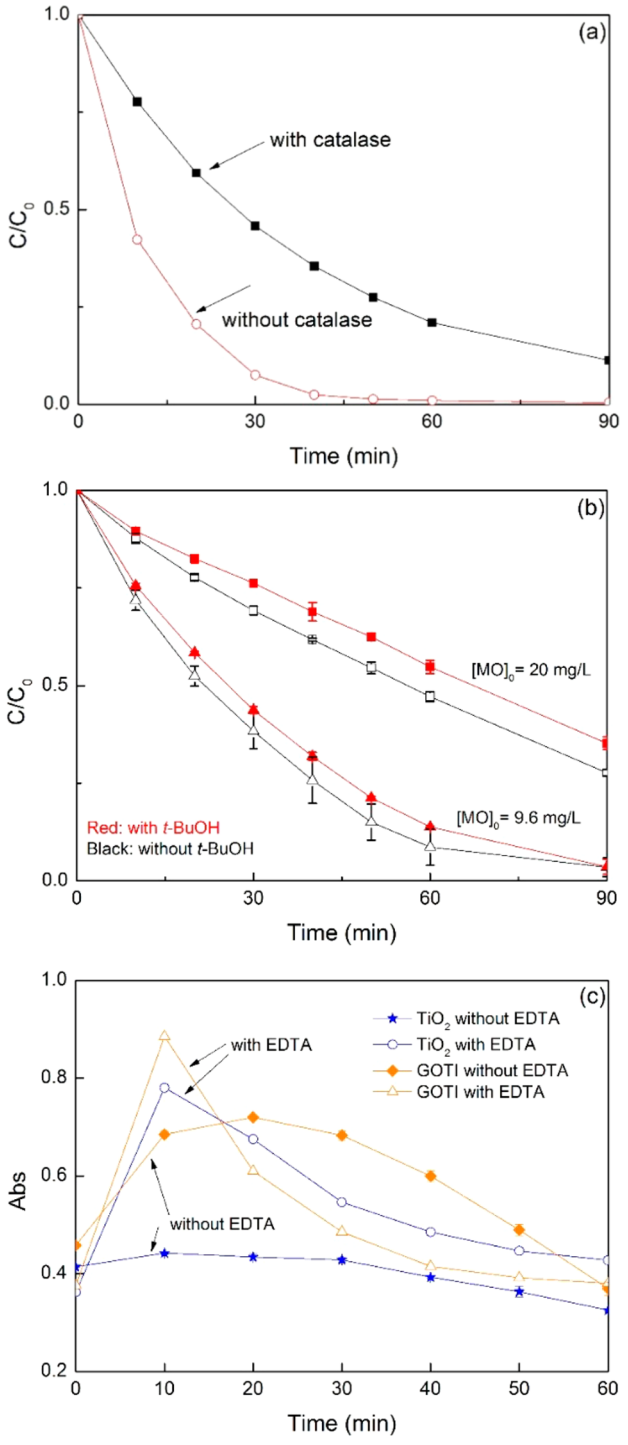

Figure 6. Photodegradation of MO in the presence of scavengers. (a) Evolution of MO concentration (C/C_0, $[MO]_0$ = 20 mg/L) with time in the presence of GOTI (16 mg/L) with/without catalase as a H_2O_2 scavenger (500 units/mL). light intensity = 18.8 mW/cm^2. (b) Evolution of MO concentration (C/C_0) with time in the presence of GOTIM-B (16 mg/L) with/without *t*-BuOH as a hydroxyl radical scavenger (10 mM). light intensity = 14.4 mW/cm^2. (c) Evolution of absorbance at 247 nm with time in the presence of GOTI (16 mg/L) with/without EDTA as a hole scavenger (4 mM). $[MO]_0$ = 20 mg/L, light intensity = 18.8 mW/cm^2.

earlier time than without EDTA, indicating increased electron availability for MO reductions. These results suggest that by controlling or scavenging holes, higher reduction performance for these materials can be achieved.

On the basis of these results, we propose two reaction pathways for photoinduced holes and electrons for the described graphene−TiO_2 nanocomposites (Figure S6, Supporting Information). Both photocatalytic oxidation and reduction pathways are possible with graphene−TiO_2-based

dx.doi.org/10.1021/am5025275 | ACS Appl. Mater. Interfaces 2014, 6, 11766−11774

photocatalysts, as described here for the case of methyl orange degradation. Enhanced photocatalytic oxidation involves both direct oxidation by holes and indirect oxidation by multiple ROS, including $OH\cdot$, $O_2^{-}\cdot$ and H_2O_2. For these materials, reactants such as methyl orange can also compete with O_2 for the reducing electrons, which subsequently leads to (direct) reductive reactions. Such pathways, increasing the production (or availability) of electrons, highlight crumpled graphene–TiO_2 as also a promising effective photocatalytic reductant with potentially wide applicability. Further, such reduction reactions can be engineered (or shifted) through depleting O_2 (or other electron scavengers) and adding hole scavengers, to affect recombination kinetics even further, thus achieving enhancement.

CONCLUSIONS

In summary, this work demonstrates the synthesis of novel ternary crumpled graphene-based nanocomposite platform materials by utilizing presynthesized nanoparticles via an aerosol route. Results clearly demonstrate significant material enhancement of TiO_2 photocatalytic performance that is in line (or better) with previously observed 2D graphene/graphene oxide composites. Moreover, as highly water stable, aggregation-resistant 3D structures, GOTIM not only maintains high surface to volume ratios (monomeric) in water, but can also be magnetically recoverable under low magnetic fields, allowing for a number of separation strategies for reuse/recycling. Further, GOTIM also demonstrates significant potential for broad photocatalytic reduction reactions, which could greatly expand the application potentials/processes considered for aqueous-based TiO_2–carbon catalysts.

ASSOCIATED CONTENT

Supporting Information

HR-TEM image, XRD patterns, and UV–vis absorption spectrum of GOTIM nanocomposites, increased light intensity on photocatalytic performance, cyclic photodegradation experiments, proposed main reaction pathways for photoinduced holes and electrons and fitting of pseudo-first-order kinetics. This material is available free of charge via the Internet at http://pubs.acs.org.

AUTHOR INFORMATION

Corresponding Authors

*Pratim Biswas. Tel: +1-314-935-5548. Fax: +1-314-935-5464. E-mail: pbiswas@wustl.edu.

*John D. Fortner. Tel: +1-314-935-9293. Fax: +1-314-935-5464. Email: jfortner@wustl.edu.

Notes

The authors declare no competing financial interest.

ACKNOWLEDGMENTS

The authors thank McDonnell Academy Global Energy and Environment Partnership (MAGEEP), Washington University in St. Louis for funding support. Electron microscopy work was performed at the Nano Research Facility (NRF) at Washington University in St. Louis, a member of the National Nanotechnology Infrastructure Network (NNIN), supported by the National Science Foundation under Grant No. ECS-0335765.

REFERENCES

(1) Wei, C.; Lin, W. Y.; Zainal, Z.; Williams, N. E.; Zhu, K.; Kruzic, A. P.; Smith, R. L.; Rajeshwar, K. Bactericidal Activity of TiO_2 Photocatalyst in Aqueous Media: Toward a Solar-Assisted Water Disinfection System. *Environ. Sci. Technol.* **1994**, *28*, 934–938.

(2) Shannon, M. A.; Bohn, P. W.; Elimelech, M.; Georgiadis, J. G.; Marinas, B. J.; Mayes, A. M. Science and Technology for Water Purification in the Coming Decades. *Nature* **2008**, *452*, 301–310.

(3) Long, Y.; Lu, Y.; Huang, Y.; Peng, Y.; Lu, Y.; Kang, S.-Z.; Mu, J. Effect of C60 on the Photocatalytic Activity of TiO_2 Nanorods. *J. Phys. Chem. C* **2009**, *113*, 13899–13905.

(4) Woan, K.; Pyrgiotakis, G.; Sigmund, W. Photocatalytic Carbon-Nanotube-TiO_2 Composites. *Adv. Mater.* **2009**, *21*, 2233–2239.

(5) Zhang, H.; Lv, X. J.; Li, Y. M.; Wang, Y.; Li, J. H. P25-Graphene Composite as a High Performance Photocatalyst. *ACS Nano* **2010**, *4*, 380–386.

(6) Luo, J.; Jang, H. D.; Sun, T.; Xiao, L.; He, Z.; Katsoulidis, A. P.; Kanatzidis, M. G.; Gibson, J. M.; Huang, J. Compression and Aggregation-Resistant Particles of Crumpled Soft Sheets. *ACS Nano* **2011**, *5*, 8943–8949.

(7) Ma, X.; Zachariah, M. R.; Zangmeister, C. D. Crumpled Nanopaper from Graphene Oxide. *Nano Lett.* **2012**, *12*, 486–489.

(8) Wang, W.-N.; Jiang, Y.; Biswas, P. Evaporation-Induced Crumpling of Graphene Oxide Nanosheets in Aerosolized Droplets: Confinement Force Relationship. *J. Phys. Chem. Lett.* **2012**, *3*, 3228–3233.

(9) Wang, Y.; Wu, Y.; Huang, Y.; Zhang, F.; Yang, X.; Ma, Y.; Chen, Y. Preventing Graphene Sheets from Restacking for High-Capacitance Performance. *J. Phys. Chem. C* **2011**, *115*, 23192–23197.

(10) Yang, X.; Zhu, J.; Qiu, L.; Li, D. Bioinspired Effective Prevention of Restacking in Multilayered Graphene Films: Towards the Next Generation of High-Performance Supercapacitors. *Adv. Mater.* **2011**, *23*, 2833–2838.

(11) Mao, S.; Wen, Z.; Kim, H.; Lu, G.; Hurley, P.; Chen, J. A General Approach to One-Pot Fabrication of Crumpled Graphene-Based Nanohybrids for Energy Applications. *ACS Nano* **2012**, *6*, 7505–7513.

(12) Chen, Y.; Guo, F.; Jachak, A.; Kim, S.-P.; Datta, D.; Liu, J.; Kulaots, I.; Vaslet, C.; Jang, H. D.; Huang, J.; Kane, A.; Shenoy, V. B.; Hurt, R. H. Aerosol Synthesis of Cargo-Filled Graphene Nanosacks. *Nano Lett.* **2012**, *12*, 1996–2002.

(13) Chen, Y.; Guo, F.; Qiu, Y.; Hu, H.; Kulaots, I.; Walsh, E.; Hurt, R. H. Encapsulation of Particle Ensembles in Graphene Nanosacks as a New Route to Multifunctional Materials. *ACS Nano* **2013**, *7*, 3744–3753.

(14) Luo, J.; Zhao, X.; Wu, J.; Jang, H. D.; Kung, H. H.; Huang, J. Crumpled Graphene-Encapsulated Si Nanoparticles for Lithium Ion Battery Anodes. *J. Phys. Chem. Lett.* **2012**, *3*, 1824–1829.

(15) Jang, H. D.; Kim, S. K.; Chang, H.; Choi, J.-W.; Luo, J.; Huang, J. One-Step Synthesis of Pt-Nanoparticles-Laden Graphene Crumples by Aerosol Spray Pyrolysis and Evaluation of Their Electrocatalytic Activity. *Aerosol Sci. Technol.* **2012**, *47*, 93–98.

(16) Jang, H. D.; Kim, S. K.; Chang, H.; Roh, K.-M.; Choi, J.-W.; Huang, J. A Glucose Biosensor Based on TiO_2–Graphene Composite. *Biosens. Bioelectron.* **2012**, *38*, 184–188.

(17) Wang, W.-N.; Jiang, Y.; Fortner, J. D.; Biswas, P. Nanostructured Graphene-Titanium Dioxide Composites Synthesized by a Single Aerosol Process for Photoreduction of Carbon Dioxide. *Environ. Eng. Sci.* **2014**, DOI: 10.1089/ees.2013.0473.

(18) Zhang, Y.; Tang, Z.-R.; Fu, X.; Xu, Y.-J. TiO_2–Graphene Nanocomposites for Gas-Phase Photocatalytic Degradation of Volatile Aromatic Pollutant: Is TiO_2–Graphene Truly Different from Other TiO_2–Carbon Composite Materials? *ACS Nano* **2010**, *4*, 7303–7314.

(19) Guo, J.; Zhu, S.; Chen, Z.; Li, Y.; Yu, Z.; Liu, Q.; Li, J.; Feng, C.; Zhang, D. Sonochemical Synthesis of TiO_2 Nanoparticles on Graphene for Use as Photocatalyst. *Ultrason. Sonochem.* **2011**, *18*, 1082–1090.

(20) Nguyen-Phan, T.-D.; Pham, V. H.; Shin, E. W.; Pham, H.-D.; Kim, S.; Chung, J. S.; Kim, E. J.; Hur, S. H. The Role of Graphene

Oxide Content on the Adsorption-enhanced Photocatalysis of Titanium Dioxide/Graphene Oxide Composites. *Chem. Eng. J.* **2011**, *170*, 226−232.
(21) Pastrana-Martínez, L. M.; Morales-Torres, S.; Likodimos, V.; Figueiredo, J. L.; Faria, J. L.; Falaras, P.; Silva, A. M. T. Advanced Nanostructured Photocatalysts Based on Reduced Graphene Oxide−TiO_2 Composites for Degradation of Diphenhydramine Pharmaceutical and Methyl Orange Dye. *Appl. Catal., B* **2012**, *123*−*124*, 241−256.
(22) Selli, E.; Eliet, V.; Spini, M. R.; Bidoglio, G. Effects of Humic Acids on the Photoinduced Reduction of U(VI) in the Presence of Semiconducting TiO_2 Particles. *Environ. Sci. Technol.* **2000**, *34*, 3742−3748.
(23) Selli, E.; De Giorgi, A.; Bidoglio, G. Humic Acid-Sensitized Photoreduction of Cr(VI) on ZnO Particles. *Environ. Sci. Technol.* **1996**, *30*, 598−604.
(24) Kyung, H.; Lee, J.; Choi, W. Simultaneous and Synergistic Conversion of Dyes and Heavy Metal Ions in Aqueous TiO_2 Suspensions under Visible-Light Illumination. *Environ. Sci. Technol.* **2005**, *39*, 2376−2382.
(25) Vinu, R.; Madras, G. Kinetics of Simultaneous Photocatalytic Degradation of Phenolic Compounds and Reduction of Metal Ions with Nano-TiO_2. *Environ. Sci. Technol.* **2007**, *42*, 913−919.
(26) Schmelling, D. C.; Gray, K. A.; Kamat, P. V. Role of Reduction in the Photocatalytic Degradation of TNT. *Environ. Sci. Technol.* **1996**, *30*, 2547−2555.
(27) Wang, W.-N.; An, W.-J.; Ramalingam, B.; Mukherjee, S.; Niedzwiedzki, D. M.; Gangopadhyay, S.; Biswas, P. Size and Structure Matter: Enhanced CO_2 Photoreduction Efficiency by Size-Resolved Ultrafine Pt Nanoparticles on TiO_2 Single Crystals. *J. Am. Chem. Soc.* **2012**, *134*, 11276−11281.
(28) Hummers, W. S.; Offeman, R. E. Preparation of Graphitic Oxide. *J. Am. Chem. Soc.* **1958**, *80*, 1339−1339.
(29) Ma, J.; Graham, N. J. D. Degradation of Atrazine by Manganese-Catalysed Ozonation-Influence of Radical Scavengers. *Water Res.* **2000**, *34*, 3822−3828.
(30) Fortner, J. D.; Kim, D.-I.; Boyd, A. M.; Falkner, J. C.; Moran, S.; Colvin, V. L.; Hughes, J. B.; Kim, J.-H. Reaction of Water-Stable C60 Aggregates with Ozone. *Environ. Sci. Technol.* **2007**, *41*, 7497−7502.
(31) Sarathy, S. R.; Mohseni, M. The Impact of UV/H_2O_2 Advanced Oxidation on Molecular Size Distribution of Chromophoric Natural Organic Matter. *Environ. Sci. Technol.* **2007**, *41*, 8315−8320.
(32) Mills, A.; Williams, G. Methyl Orange as a Probe of the Semiconductor-Electrolyte Interfaces in CdS Suspensions. *J. Chem. Soc., Faraday Trans. 1* **1987**, *83*, 2647−2661.
(33) Li, D.; Muller, M. B.; Gilje, S.; Kaner, R. B.; Wallace, G. G. Processable Aqueous Dispersions of Graphene Nanosheets. *Nat. Nanotechnol.* **2008**, *3*, 101−105.
(34) Williams, G.; Seger, B.; Kamat, P. V. TiO_2-Graphene Nanocomposites. UV-Assisted Photocatalytic Reduction of Graphene Oxide. *ACS Nano* **2008**, *2*, 1487−1491.
(35) Muszynski, R.; Seger, B.; Kamat, P. V. Decorating Graphene Sheets with Gold Nanoparticles. *J. Phys. Chem. C* **2008**, *112*, 5263−5266.
(36) Yang, X.; Zhang, X.; Ma, Y.; Huang, Y.; Wang, Y.; Chen, Y. Superparamagnetic Graphene Oxide-Fe_3O_4 Nanoparticles Hybrid for Controlled Targeted Drug Carriers. *J. Mater. Chem.* **2009**, *19*, 2710−2714.
(37) Chandra, V.; Park, J.; Chun, Y.; Lee, J. W.; Hwang, I.-C.; Kim, K. S. Water-Dispersible Magnetite-Reduced Graphene Oxide Composites for Arsenic Removal. *ACS Nano* **2010**, *4*, 3979−3986.
(38) Larciprete, R.; Fabris, S.; Sun, T.; Lacovig, P.; Baraldi, A.; Lizzit, S. Dual Path Mechanism in the Thermal Reduction of Graphene Oxide. *J. Am. Chem. Soc.* **2011**, *133*, 17315−17321.
(39) Park, S.; Dikin, D. A.; Nguyen, S. T.; Ruoff, R. S. Graphene Oxide Sheets Chemically Cross-Linked by Polyallylamine. *J. Phys. Chem. C* **2009**, *113*, 15801−15804.
(40) Sakthivel, S.; Kisch, H. Daylight Photocatalysis by Carbon-Modified Titanium Dioxide. *Angew. Chem., Int. Ed.* **2003**, *42*, 4908−4911.
(41) Chen, D.; Zhang, H.; Liu, Y.; Li, J. Graphene and Its Derivatives for the Development of Solar Cells, Photoelectrochemical, And Photocatalytic Applications. *Energy Environ. Sci.* **2013**, *6*, 1362−1387.
(42) Li, W.; Li, D.; Xian, J.; Chen, W.; Hu, Y.; Shao, Y.; Fu, X. Specific Analyses of the Active Species on $Zn_{0.28}Cd_{0.72}S$ and TiO_2 Photocatalysts in the Degradation of Methyl Orange. *J. Phys. Chem. C* **2010**, *114*, 21482−21492.
(43) Brown, G. T.; Darwent, J. R. Photoreduction of Methyl Orange Sensitized by Colloidal Titanium Dioxide. *J. Chem. Soc., Faraday Trans. 1* **1984**, *80*, 1631−1643.
(44) Jiang, G.; Lin, Z.; Chen, C.; Zhu, L.; Chang, Q.; Wang, N.; Wei, W.; Tang, H. TiO_2 Nanoparticles Assembled on Graphene Oxide Nanosheets with High Photocatalytic Activity for Removal of Pollutants. *Carbon* **2011**, *49*, 2693−2701.
(45) Yu, L.; Xi, J.; Li, M.-D.; Chan, H. T.; Su, T.; Phillips, D. L.; Chan, W. K. The Degradation Mechanism of Methyl Orange Under Photo-Catalysis of TiO_2. *Phys. Chem. Chem. Phys.* **2012**, *14*, 3589−3595.
(46) Wood, P. M. The Two Redox Potentials for Oxygen Reduction to Superoxide. *Trends Biochem. Sci.* **1987**, *12*, 250−251.
(47) Deo, M.; Shinde, D.; Yengantiwar, A.; Jog, J.; Hannoyer, B.; Sauvage, X.; More, M.; Ogale, S. Cu_2O/ZnO Hetero-Nanobrush: Hierarchical Assembly, Field Emission and Photocatalytic Properties. *J. Mater. Chem.* **2012**, *22*, 17055−17062.